Impact of wetting and drying cycles on soil structure dynamics

Julius Diel[1], Hans-Jörg Vogel[1,2], Steffen Schlüter[1*]

1. Department of Soil System Sciences, Helmholtz-Centre for Environmental Research – UFZ, Halle Germany

2. Institute of Soil Science and Plant Nutrition, Martin Luther University of Halle-Wittenberg, Halle, Germany

*corresponding author (steffen.schlueter@ufz.de)

Highlights:

- 3D crack dynamics in structured soil during WD cycles observed with X-ray CT
- Soil structure dynamics measured via structure labeling with garnet particles
- Soil structure dynamics dependent on, bulk density, SOM and clay content
- Higher SOM content led to a higher density of cracks with smaller aperture
- Soil structure dynamics is negligible due to reactivation of old cracks

Abstract
Soil structure is not static but undergoes continuous changes due to a wide range of biotic and abiotic drivers such as bioturbation and the mechanical disturbance by tillage. This continuous alteration of soil structure beyond the pure swelling and shrinking of some stable structure is what we refer to as soil structure dynamics. It has important consequences for carbon turnover in soil as it controls how quickly soil organic matter gets occluded from or exposed to mineralization. So far there are hardly any direct observations of the rate at which soil pores are formed and destroyed.

Here we employ are recently introduced labeling approach for soil structure that measures how quickly the locations of small garnet particles get randomized in soil as a measure for soil structure dynamics. We investigate the effect of desiccation crack dynamics on pore space attributes in general and soils structure turnover in particular using X-ray microtomography for repeated wetting-drying cycles. This is explored for three different soils with a range of soil organic matter content, clay content and different clay mineralogy that were sieved to a certain aggregate size fraction (0.63-2 mm) and repacked at two different bulk density levels.

The total magnitude of desiccation crack formation mainly depended on the clay content and clay mineralogy. Higher soil organic matter content led to a denser crack pattern with smaller aperture. Wetting-drying cycles did not only effect visible macroporosity (>8µm), but also unresolved mesoporosity. The changes in macroporosity were higher at lower bulk density. Most importantly, repeated wetting-drying cycles did not lead to a randomization of distances between garnet particles and pores. This demonstrates that former failure zones are reactivated during subsequent drying cycles. Hence, wetting-drying resulted in reversible particle displacement and therefore would not have triggered the exposure of occluded carbon that was not already exposed during the previous drying event.

Keywords: Soil structure; Desiccation cracks; X-ray tomography; Macropores; Clay mineralogy; Carbon turnover

Introduction
Soil structure is an important indicator of the ecological status of soil as it both controls many ecosystem functions of soil and is shaped by them (Rabot et al., 2018; Young, 2004). It defines the pathways for water and nutrient fluxes (Jarvis, 2007; Köhne et al., 2009), shapes microhabitats in soil (Baveye et al., 2018; Bottinelli et al., 2015; Young et al., 2008) and controls the micro-environmental conditions for chemical reaction patterns in soil (Totsche et al., 2018; Wilcke and Kaupenjohann, 1997). The spatial distribution of substrate and structure-mediated pathways of oxygen diffusion exert a major control on aerobic and anaerobic soil respiration (Keiluweit et al., 2017; Kuzyakov and Blagodatskaya, 2015; Smith et al., 2003) and is considered as one of the major factors controlling long-term carbon stabilization in soil (Kravchenko and Guber, 2017; Lehmann and Kleber, 2015).

Soil structure can in the broadest sense be defined as the spatial heterogeneity of the different components or properties of soil (Dexter, 1988). There are two approaches to characterize soil structure (Rabot et al., 2018). One is centered on the structure of solid components and usually focused on aggregates as the building blocks of soil. The other is focused on the pore perspective and explores the spatial arrangement of voids in undisturbed soil. This dichotomy is particularly relevant with respect to soil structure dynamics by biotic and abiotic agents which typically manifests itself through the steady formation and destruction of pores, but not of solid particles. Furthermore, soil structure dynamics might not even be detectable based on standard measures of the pore structure such as porosity and pore size distribution, since these macroscopic measures may stay constant in dynamic equilibrium, when the microscopic destruction and formation of pores are in balance. In order to resolve this problem a structure labeling approach was recently proposed that enables a direct estimation of soil structure dynamics with a combination of X-ray microtomography and a novel structure labelling approach.(Schlüter and Vogel, 2016). Aggregates are coated with small, inert garnet particles. Garnet is an iron-bearing mineral that evokes good X-ray contrast. The garnet particles are in direct contact with inter-aggregate pores after coating, except for those that get occluded in the contact area of adjacent aggregates after repacking. This results on average in shorter distances between garnet particles and nearest pores than the distance of arbitrary soil matrix locations and nearest pores. This represents an analogy to pool dilution experiments to measure carbon turnover with stable isotopes. The “short distance pool” is highly enriched in garnet particles and soil structure dynamics, or soil structure turnover as it was coined in Schlüter and Vogel (2016), will lead to a dilution of this pool by randomization of distances between garnet particles and pores through the formation of new uncoated pores or occlusion of particles through the destruction of old pores Soil structure dynamics measured by this randomization of passively translocated garnet particles has direct consequences for soil carbon turnover as the formation of new pores may expose previously occluded organic matter, which is one main explanation for the so-called Birch effect (Borken and Matzner, 2009; Lopez-Sangil et al., 2018; Navarro-García et al., 2012) Likewise, the destruction of pores may protect organic matter in its vicinity against mineralization (Beylich et al., 2010; Haas et al., 2016). It was demonstrated that compaction, a typical abiotic structure-changing process does not lead to a randomization of particle locations (Schlüter and Vogel, 2016). The “tracer particle”-pore distances increase through compaction, but this is the same for any location within the soil. Therefore it was hypothesized that other structure-forming processes may be more efficient to induce structure dynamics in the sense of its reorganization with time measured by the randomization of “tracer particle”-pore distances. In this paper, crack dynamics through wetting-drying cycles are investigated as another important abiotic process that is known to modify soil structure.

Crack dynamics mainly depend on the clay content and its mineralogy, as some minerals (i.e. kaolinite or illite) have low to no swelling potential, while this is high for others (i.e. smectite, vermiculite). A second important factor is the heterogeneity in the assembly of soil particles, as more heterogeneous soil matrices tend to crack more easily, e.g.(Fiès and Bruand, 1998; Wang et al., 2018). The aperture and width of cracks are governed by the initial water content, the drying intensity and the antecedent moisture regime. Other important factors are bulk density, the content of soil organic matter (SOM), particulate organic matter (POM), and sesquioxides (Peng et al., 2007; Tang et al., 2011, Zhang et al., 2016). However, studies regarding crack dynamics in soil often evaluate two-dimensional crack patterns in drying soil suspensions and are seldom carried out in intact, structured soils as three-dimensional crack patterns are hard to investigated in opaque media. Here, X-ray tomography provides an opportunity to study crack dynamics through non-invasive imaging. The objectives of this paper are two-fold. First, the capacity of repeated wetting-drying cycles to induce soil structure changes in general and soil structure dynamics in terms of particle-pore distances in particular are investigated. Second, the effect of important soil properties like texture, bulk density, soil organic matter content and clay mineralogy on soil structure changes through wetting-drying cycles is explored.

Materials and Methods

We examined three top soils from Germany, which differ in texture, organic matter content and clay mineralogy. The luvisol from Bad Rotthalmünster (RM) has both low clay and low SOM content (Kögel-Knabner et al., 2008), the chernozem from Bad Lauchstädt (BL) has low clay and medium SOM content (Altermann et al., 2005), and the gleysol soil from Giessen (GI) has both high clay and SOM content (Jürgen Böttcher, personal communication) (Table 1). The BL and RM soil are not only similar in terms of texture, but also in terms of clay mineralogy with volume fractions in the order of illite > kaolinite > vermiculite (Dreibrodt et al., 2002, Reinhold Jahn, personal communication). The GI soil in turn has the highest swelling capacity with vermiculite > vermiculite-illite interstratifications = illite > chlorite = kaolinite (Klaus Kaiser, personal communication). As a consequence of different SOM contents and clay mineralogy the three soils all form different two-dimensional crack patterns, as demonstrated in Figure 1. These crack patterns evolved from soil emulsions composed of 50 cm^3 soil and 30 cm^3 water that dried in petri dishes to a final soil height of ~ 3 mm through evaporation at room temperature. The main difference is the separation distance between cracks, which seems to decrease with increasing SOM content.

Table 1: Main characteristics of the investigated soils.

soil	clay [%]	silt [%]	texture WRB	SOM [%]	C:N
Bad Rotthalmünster (RM)	16	73	Silty loam	1.29	9.6
Bad Lauchstädt (BL)	21	68	Silty loam	2.05	10.08
Giessen (GI)	27	41	Clay loam	4.46	9.95

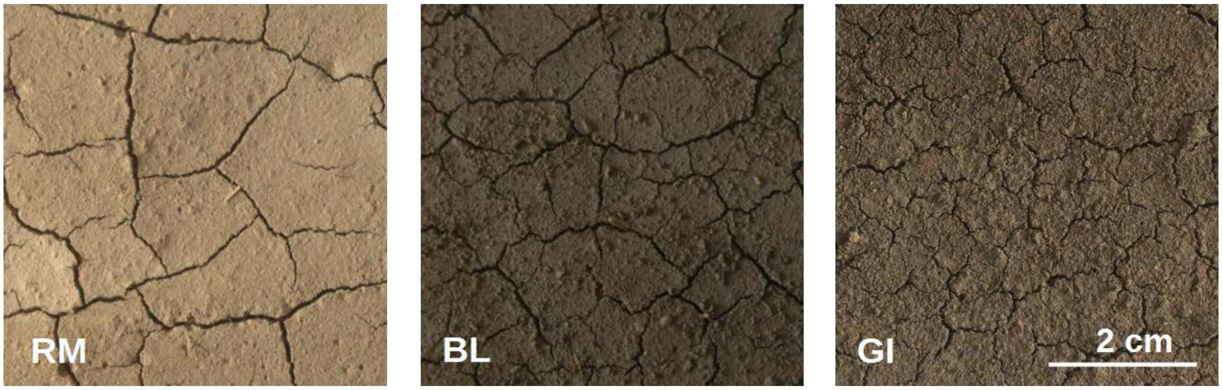

Figure 1: Two-dimensional crack patterns of the investigated soils in air-dried soil suspensions.

Sample preparation: Sieving, Coating, Packing

The sample preparation is similar to Schlüter and Vogel (2016). Dry soil is passed through sieves of 0.63 and 2 mm mesh size, moistened on wet paper towel, coated with garnet particles (size: 45-100µm, Garnit #240, Kuhmichel Abrasiv GmbH, Ballenstedt, Germany) and filled into 5 ml syringes, which were densely perforated to ensure a uniform drying. Inside the syringes, the aggregates were compacted to two bulk densities (Bd1: 1.22 ± 0.03 g/cm³, Bd2: 1.48 ± 0.05 g/cm³) through uniaxial compaction from the top with a piston.

Wetting/Drying protocol

The bottom of the syringes was connected to a water reservoir to adjust the matric potential h_m to a wet state of -25cm with a hanging water column. One day after wetting, the samples were scanned for the first time (W1) and then disconnected from the water reservoir to let the soil dry out by evaporation. Each day the weight of each sample was measured. After roughly one week the weight of the sample converged to a final value and its dry state (D1) was scanned, before the cycle was repeated (W2 and D2 respectively). In total, this amounts to 24 different combinations of soils, bulk densities and moisture states with five replicated samples each.

X-ray tomography and image analysis

X-ray tomographs were acquired with a X-TEk XCT 225 (Nikon Metrology) at an energy of 110 kV and beam current of 100 µA with 2300 projections and 2 projections per second. The projections were reconstructed into a 3D tomogram with a filtered back-projection algorithm implemented in the 3D CT-Pro software (Nikon Metrology) with a resolution of 8µm and a grayscale depth of 8-bit. To achieve optimal contrast in the soil matrix, the 1% and 99% percentile of the darkest and brightest voxels were set to 0 and 255, respectively. This linear contrast enhancement allows for a quantitative comparison of matrix gray values as explained below.

Image processing

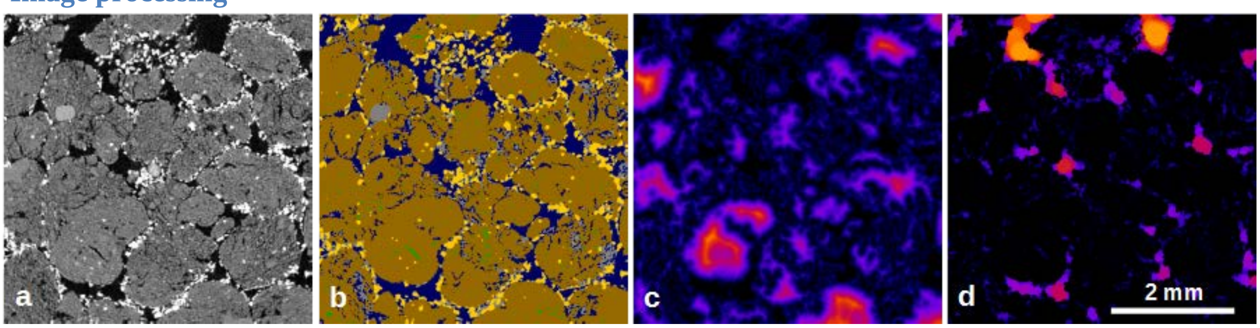

Figure 2: Steps of the image processing illustrated for a two-dimensional section. a) X-ray CT with original grayscale, b) segmented image with colors representing soil (brown), connected pores (blue), occluded pores (green), garnet particles (yellow), dense large stones (gray), c) Euclidean distance of any soil pixel to the next connected pore, d) Local pore size.

Image processing was carried out according to previously introduced protocols (Schlüter and Vogel, 2016; Schlüter et al., 2014). A short graphic overview is given in Figure 2.Pores, soil matrix and dense large stones were identified via thresholding of the gray scale data after noise removal with a 2D non-local means filter (Darbon et al., 2008) distributed as a Fiji plugin with the same name by the biomedgroup update site in Fiji/ImageJ (Schindelin et al., 2012). Thresholding into these three classes was carried out with the average of five different histogram-based threshold detection methods after outlier removal (Schlüter et al., 2014) as implemented in QuantIm (available at www.quantim.ufz.de). For some combinations of bulk densities and soils only one out of five methods was chosen (Kittler and Illingworth, 1986), as the failure of several others also biased the average. Garnet particles constitute the fourth material class. These were detected separately via feature detection using the 2nd derivative of gray values (Laplacian) after Gaussian smoothing with three different radii of the Gaussian filter kernel (σ=

[8,16,24] µm) as implemented in the FeatureJ plugin in Fiji (© Erik Meijering).. The different σ values are meant to cover the actual size range of particles. Spherical particles with a corresponding radius evoke very negative intensities in the Laplacian. The absolute intensities in the Laplacian images decrease with increasing σ^2 so they need to be normalized before they are merged together with the minimum (most negative) gray values out of three Laplacians. This single image is then segmented into particles and background via Hysteresis thresholding with manually defined thresholds implemented in the 3D ImageJ Suite plugin (Ollion et al., 2013). Finally, a fifth material class is created by dividing the pore class into connected pores and isolated pores occluded in aggregates using a size criterion of 10000 voxels (0.005 mm³) which is implemented in the MorpholibJ plugin in Fiji (Legland et al., 2016). The final segmentation results are shown in Figure 2(c). Additional information about the workflow is presented in Schlüter and Vogel (2016).

. The segmented images were analyzed in different directions. First, the Euclidean distance of any non-pore voxel to the closest connected pore voxel was computed (Figure 2c). The first central moment of this pore distance distribution serves as an estimate of the average pore distance in soil. Second, the pore size distribution (Figure 2d) was calculated with the maximum inscribed sphere method. The first central moment of this pore size distribution is an estimate of the average pore diameter (Local Thickness in Fiji). Finally, the dimensionless connectivity indicator Γ (Renard and Allard, 2013) was calculated based on pore cluster labelling in MorpholibJ (Legland et al., 2016),

$$\Gamma = \sum_{i=1}^{n} x_i^2 / (\sum_{i=1}^{n} x_i)^2$$

where n is the number of pore clusters and x_i is the volume of pore cluster i, so that $\Gamma = 1$ for a completely connected pore network and Γ approaches zero for a very fragmented pore network.

Statistical analysis

Mean values of soil structural attributes were tested for significant differences ($p<0.05$) between combinations of bulk density and moisture states using Tukey's HSD test in the agricolae package in R (de Mendiburu, 2019). Prior it was asserted visually that the residuals are distributed normally.

Results

Visual assessment

At the low bulk density (Bd1), inter-aggregate pores are clearly visible in the wet stage (W2) (Figure 3). This means that a large part of the garnet particles is in direct contact with connected pores. The structural changes through drying (W2→D2) can be recognized very well in the segmented images. The difference in connected porosity between the two moisture levels seems to increase in the order RM < BL < GI. The proportion of pores classified as occluded is relatively small.

At the high bulk density Bd2, there are almost no inter-aggregate pores at the second wetting stage (W2) in all three soils (Figure 3). The former aggregate boundaries can still be identified by the lined up, occluded garnet particles. When these densely packed soils dry out again (D2), the amount of additional connected pores differs again between soils. In RM soil, existing cracks expand slightly, but new cracks are hardly formed. In GI soil, a lot of very small cracks occur when dry. The dynamics in BL soil are somewhere in between. These observations are in line with crack patterns in unstructured emulsions (Figure 1).

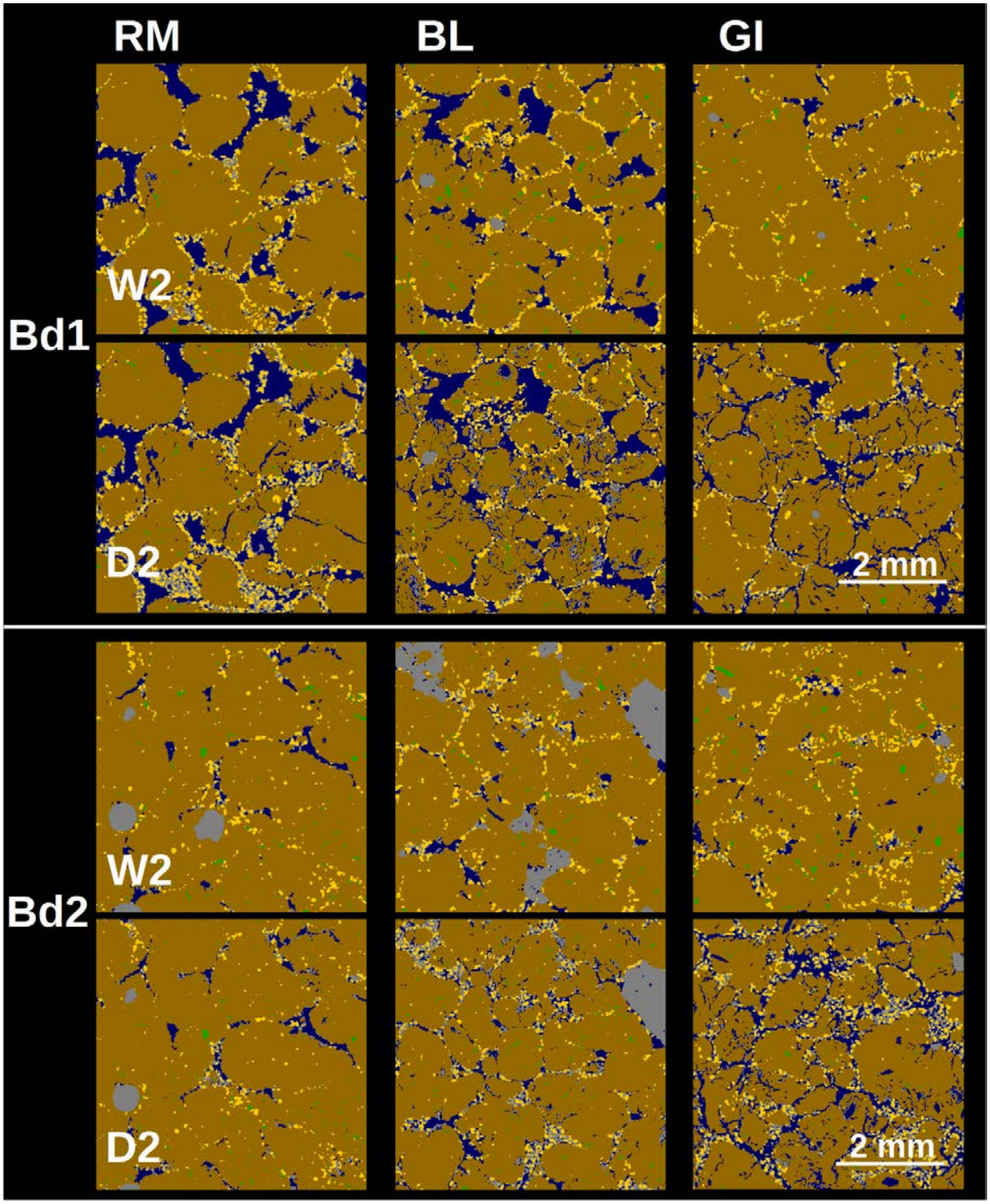

Figure 3: Two-sections of the segmented X-ray CT images for each soil and bulk density. Brown: Soil, Blue: Air, Green: Occluded pores, Yellow: Garnet particles, Gray: Unclassified / masked. The shown images are from the second wet and dry cycle each.

Soil matrix density

The average gray value of the soil matrix class corresponds to the mean X-ray attenuation in arbitrary units that is bounded by the average attenuation of air and garnet after reconstruction with the percentile method. This gray value depends on the local electron density which may increase with increasing bulk density through shrinkage (mineral matter per voxel grows on the expense of air and water) or with increasing water content through wetting (water content per voxel grows on the expense of air content). Which of the two counter-acting effects dominates depends on the soil properties (Figure 4,Table 2). In GI soil with a large amount of swelling clay minerals the contraction upon drying always leads to significantly higher matrix density in the dry state irrespective of initial bulk density. Moreover, the changes in attenuation are very reversible. In the other two soils the changes are less reversible between the first and second WD-cycle. The BL soil with lower bulk density (Bd1) behaves similar to the GI soil. Here, again soil contraction during drying leads to the highest gray levels at D1 and D2, though the difference to the matrix density at W2 is not significant due to high standard deviations and small sample number (n=5). The trend is reversed at the higher bulk density (Bd2). Here the high initial compaction and the lower shrinking capacity limit the susceptibility to contraction so that the added X-ray attenuation by water leads to the highest X-ray attenuation at W2. The RM soil with the lowest SOM content is the only soil with a significant difference of average matrix gray values between Bd1 and Bd2. That is, the higher compaction does not only lead to a difference in visible porosity, but also to less unresolved mesoporosity. There is no consistent trend in matrix gray value with water content changes at Bd1. At Bd2, the RM soil behaves similar to the BL soil with the highest matrix gray values in the wet state (W2) due to the added X-ray attenuation by water. Again the differences between moisture states are not significant due to high stand deviations.

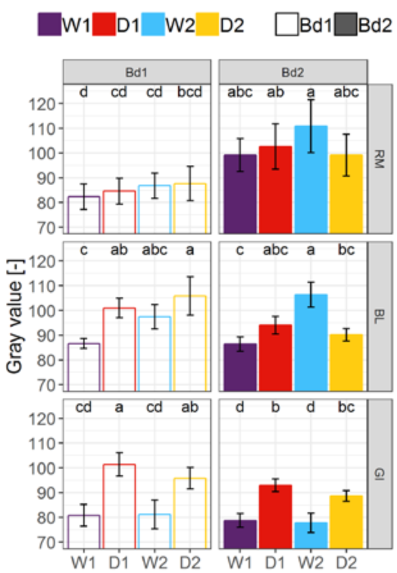

Figure 4: Average gray values of the soil matrix for each variant (soil, bulk density and moisture; n=5). Significant differences (p<0.05) among combinations bulk densities and moisture states are indicated by different letters.

Table 2: Table of means and standard deviations of soil structure attributes (n=5). Different letters in superscript indicate significant differences ($p<0.05$) among combinations of bulk density and moisture states tested independently for each soil..

			Matrix gray value [-]		Porosity [%]		Pore diameter [µm]		Gamma-connectivity [%]		soil pore distance [µm]		particle pore distance [µm]	
soil	bulk density	variant	avg	sd	avg	sd	avg	sd	avg	sd	avg	sd	avg	sd
BL	Bd1	D1	101.0^{ab}	3.9	22.8^{a}	2.5	82.2^{a}	6.3	94.6^{a}	2.1	64.6^{d}	4.1	24.9^{c}	1.7
		D2	105.8^{a}	7.8	22.9^{a}	1.8	87.1^{a}	5.0	94.7^{a}	1.8	68.7^{d}	8.6	27.1^{c}	2.7
		W1	86.6^{c}	1.9	14.3^{a}	2.1	81.5^{a}	8.6	88.2^{a}	8.6	108.4^{cd}	5.6	50.1^{bc}	9.1
		W2	97.4^{abc}	4.9	14.5^{a}	1.9	80.2^{a}	3.9	86.1^{a}	8.9	101.9^{cd}	5.8	52.0^{bc}	5.8
	Bd2	D1	94.0^{abc}	3.5	4.6^{bc}	1.2	34.2^{bc}	3.4	22.2^{bc}	20.8	120.2^{bc}	27.8	63.1^{bc}	22.2
		D2	90.2^{ab}	2.5	5.1^{c}	1.1	33.1^{c}	2.9	29.6^{b}	20.5	104.2^{cd}	18.9	48.4^{bc}	14.4
		W1	86.4^{c}	2.9	2.5^{bc}	0.2	38.3^{bc}	3.8	0.2^{c}	0.1	164.3^{b}	29.3	92.6^{b}	27.9
		W2	106.4^{a}	5.0	2.3^{b}	0.2	48.3^{b}	9.4	0.2^{c}	0.1	215.8^{a}	31.2	168.1^{a}	34.1
GI	Bd1	D1	101.4^{a}	4.7	23.5^{a}	2.5	78.8^{a}	9.3	95.9^{a}	1.3	61.0^{de}	9.2	30.9^{cd}	6.6
		D2	95.8^{ab}	4.3	24.7^{a}	1.8	74.0^{a}	8.3	96.7^{a}	0.8	51.8^{e}	5.3	24.4^{d}	2.8
		W1	80.8^{cd}	4.4	9.3^{cd}	2.0	53.3^{b}	6.8	73.4^{ab}	13.8	120.3^{cd}	20.4	65.8^{cd}	18.9
		W2	81.2^{cd}	5.8	8.5^{d}	3.4	58.1^{b}	7.7	47.7^{a}	31.7	137.6^{bc}	39.7	89.1^{bc}	35.7
	Bd2	D1	93.0^{b}	2.5	13.6^{bc}	3.0	54.3^{b}	7.5	83.3^{b}	9.6	75.5^{de}	21.9	45.5^{cd}	17.1
		D2	88.6^{bc}	2.2	15.2^{b}	2.6	50.7^{bc}	5.9	88.8^{ab}	5.5	59.1^{e}	10.5	31.1^{cd}	7.0
		W1	78.8^{d}	2.8	2.5^{e}	1.1	39.3^{c}	3.8	0.6^{c}	0.5	198.1^{a}	40.1	150.5^{a}	41.0
		W2	77.8^{d}	3.9	3.4^{e}	1.1	37.9^{c}	3.1	4.2^{c}	8.5	182.9^{ab}	38.2	135.2^{ab}	37.6
RM	Bd1	D1	84.6^{cd}	5.2	19.8^{ab}	1.6	85.0^{a}	6.8	92.2^{a}	2.8	73.5^{d}	9.2	28.8^{c}	1.6
		D2	87.6^{bcd}	6.9	21.2^{a}	0.9	91.2^{a}	8.3	93.0^{a}	2.0	74.6^{d}	12.6	29.7^{c}	2.9
		W1	82.4^{d}	5.1	16.3^{bc}	2.5	87.6^{a}	9.6	86.4^{a}	7.3	107.6^{d}	25.4	45.1^{c}	18.3
		W2	86.8^{cd}	5.1	15.1^{c}	2.1	88.7^{a}	5.4	87.4^{a}	4.3	111.4^{d}	23.5	50.6^{c}	15.9
	Bd2	D1	102.6^{ab}	9.1	3.7^{d}	0.7	37.7^{b}	6.3	17.9^{bc}	15.6	163.9^{bc}	15.9	115.0^{b}	12.3
		D2	99.2^{abc}	8.4	3.8^{d}	0.8	34.2^{b}	5.7	19.4^{b}	16.2	154.6^{c}	14.4	102.3^{b}	11.7
		W1	99.2^{abc}	6.6	2.2^{d}	0.6	40.3^{b}	4.9	0.3^{c}	0.3	214.6^{a}	27.4	160.9^{a}	22.8
		W2	110.8^{a}	10.7	3.0^{d}	1.0	43.4^{b}	5.5	3.6^{bc}	6.9	201.8^{ab}	29.5	153.4^{a}	24.8

Macroporosity profiles

The three soils clearly show different shrinking and swelling behavior not only in terms of unresolved porosity (Figure 4) but also with respect to visible porosity, depicted as macroporosity profiles (Figure 5, Table 2). All soils have in common that there is a gradual increase in macroporosity towards the bottom because the compaction is carried out at the top. Moreover, all soils at both bulk densities have in common that macroporosity increases as the soils dry out. However, the magnitude is larger at lower bulk densities. Apparently, at a lower bulk density there are more desiccation cracks or pre-existing unresolved pores that become big enough in a dry state to be resolved at a nominal resolution of 8µm. The gain in macroporosity by drying is very different for the three soils and increases in the order of RM<BL<GI. The GI soil with the highest proportion of swelling clay minerals even has a higher reduction in macroporosity by rewetting than by compaction from Bd1 to Bd2.

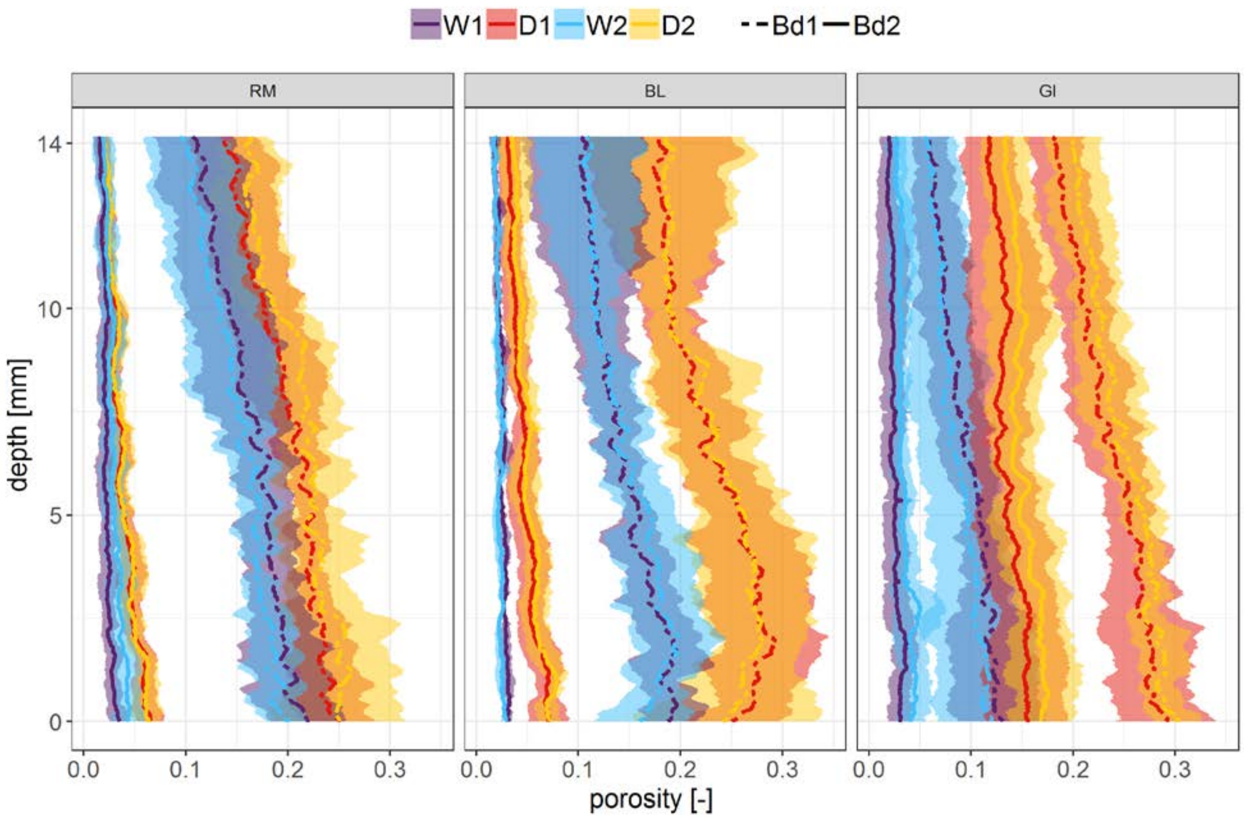

Figure 5: Porosity profile for each variant (soil, bulk density and moisture). Transparent areas represent standard deviation (n=5).

Pore diameter vs macroporosity

An increase in macroporosity through the formation of desiccation cracks may lead to an increase in the average pore diameter of visible pores through an increase in crack aperture everywhere. However this might be compensated by the emergence of small cracks that were not visible in a wet state. Which of the two effects dominate depends on the soil and bulk density (Figure 6, Table 2). In the GI soil the increase in crack aperture dominates at both bulk densities, hence the dry samples have a significantly higher average pore diameter. In the RM and BL soil at the lower bulk density (Bd1) both effects cancel each other out, whereas at the higher bulk density the reduction in average pore diameter caused by the emergence of small desiccation cracks slightly dominates, which leads to a small decrease through drying.

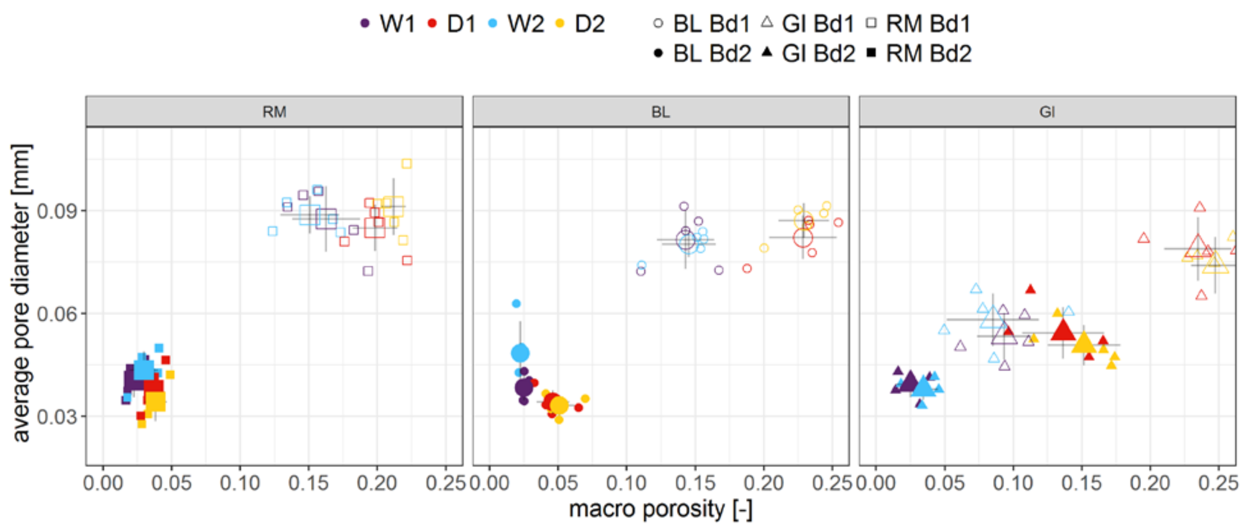

Figure 6: Average pore diameter as a function of visible porosity for all soils, bulk density and moistures. Large symbols with cross hairs represent averages and standard deviations. Small symbols represent individual samples.

Pore connectivity

The reduction in pore connectivity estimated by the Γ indicator with decreasing macroporosity is highly non-linear (Figure 7). There is a steep decline in this connection probability for all three soils in a narrow range of 0.04-0.1. At higher macroporosities (mostly Bd1 and/or dry samples) the pore network is dominated by one connected cluster, whereas at lower macroporosities (mostly wet BD2 samples) it falls apart into many isolated pore clusters. Hence the general shape seems to be enforced by the sieving and packing procedure. Small changes in the critical macroporosity range emerge for different soils, e.g. the lowest Γ values for GI+Bd1+W2 (blue empty triangles) seem to stem from small, emerging desiccation cracks which are not connected to the dominating pore cluster so that the Γ values are smaller as compared to other soils in the same macroporosity range that have a lower mass fraction of swelling clay minerals.

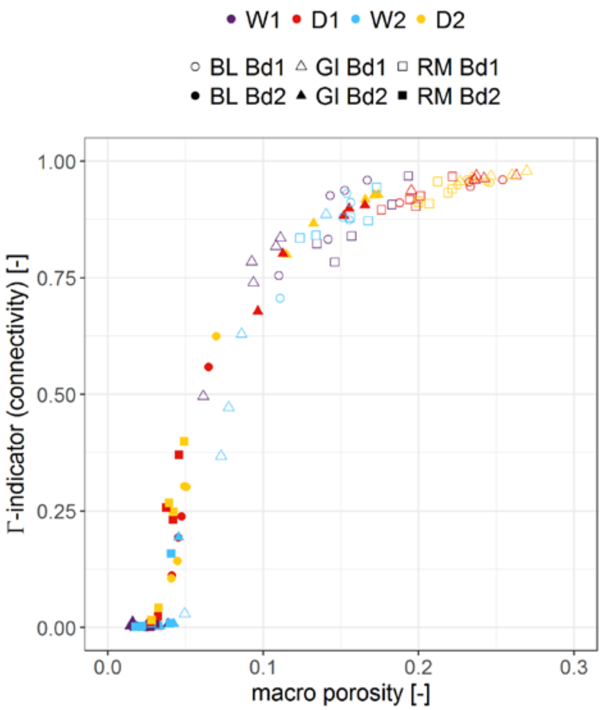

Figure 7: Connectivity indicator Γ of the pore system as a function of visible porosity for all soils, bulk density and moistures.

Pore distance metrics

The mean pore distance in bulk soil decreases non-linearly with increasing macroporosity (Figure 8)The average distance from a soil matrix voxel to the closest connected pore voxel increases, when there are less visible pores, and vice versa. The general shape of the relationship and the absolute values (Table 2) are similar for all three soils, in particular for low (<0.1) and high macroporosities (>0.2). This similarity is apparently imposed by the sieving and packing protocol. There are differences in the mean pore distance in bulk soil at intermediate macroporosity, e.g. a decrease from 0.11 mm for RM+Bd1+W2 to 0.06 mm for GI+Bd2+D2 at the same macroporosity around 0.15. That is, the even distribution of desiccation cracks in the dry GI soil leads to shorter average soil-pore distances than the larger, but fewer inter-aggregate pores of the wet RM soil (compare Figure 8, insets).

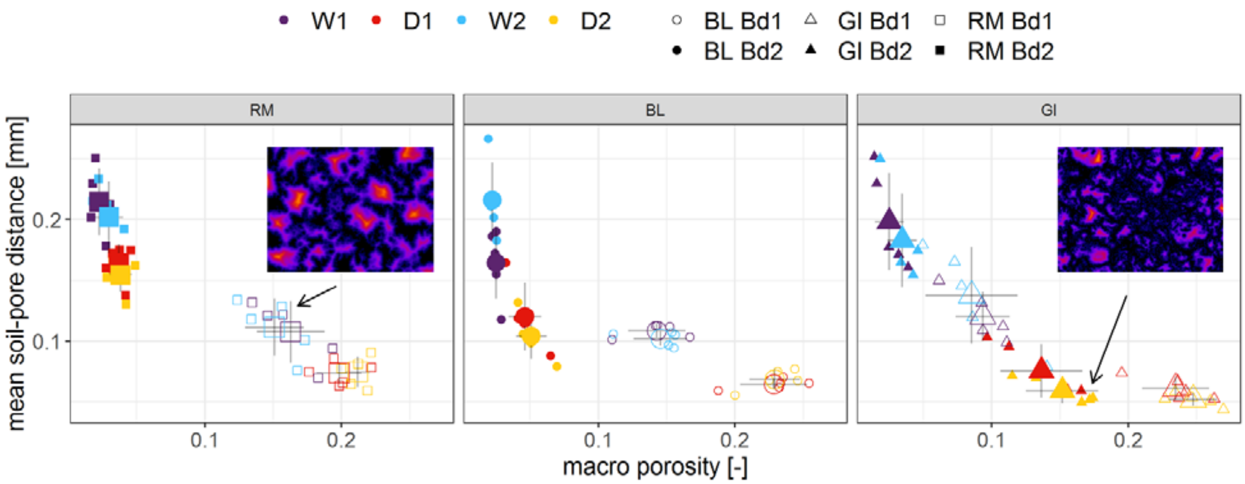

Figure 8: Mean soil-pore distance [mm] as a function of macroporosity [-].The insets show a 2D section of pore distances in a RM+Bd1+W2 and GI+Bd2+D2sample (brighter means higher distance, pores are black)

The frequency distributions of soil-pore distances are shown as supporting information (Fig S1) together with the frequency distributions of garnet particle-pore distances. The mean bulk soil-pore distance and garnet particle-pore distances which are derived from these distributions are shown in Figure 9. For all soils, bulk densities and moisture states the particles have shorter distances to the connected pore space than the average soil voxel. Particles get occluded in the soil matrix through rewetting so that the average garnet particle-pore distance increases, but so does the average bulk soil-pore distance in general. Two wetting-drying cycles do not bring the distances closer to the 1:1 line. This only seems to happen at the highest macroporosities. However, this is an artifact of the finite size of particles. That is, the bulk soil-pore distances decrease substantially and nearly all garnet particles are exposed to connected pores, but the average particle-pore distances cannot decrease beyond the particle radius of 0.02 - 0.03 mm.

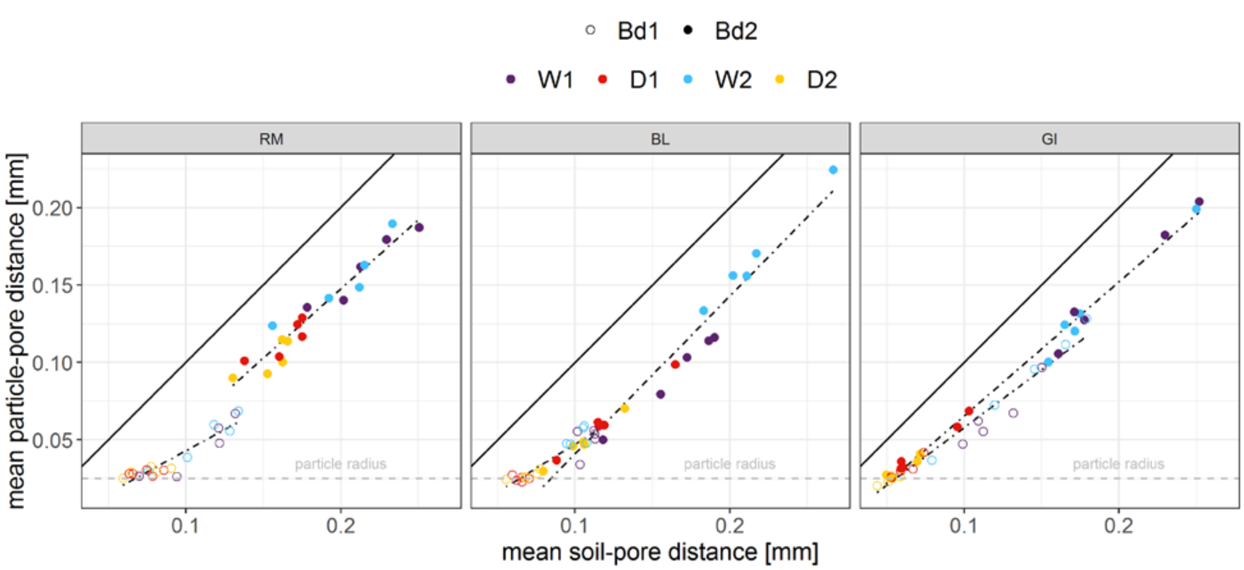

Figure 9: Mean particle-pore distance as a function of mean soil-pore distance for all soils, bulk densities and moisture states including linear regression models for each bulk density.

Discussion

Impact of soil properties on pore space dynamics

The three soils were chosen such that the impact of texture, SOM content and clay mineralogy on structure dynamics during desiccation and rewetting could be investigated. The initial pore structure prior to the first wetting (W1) is roughly the same for all soils due to identical sieving and packing. The main difference between the luvisol (RM) and the chernozem (BL) is a higher SOM content in the BL soil which entailed a larger increase in macroporosity through drying especially at the low bulk density (1.22g/cm³, Bd1) but also at the higher bulk density (1.48g/cm³, Bd2). A visual assessment of both the dried emulsions and structured soils demonstrate that the RM soil with low SOM content tend to create a sparse network of large desiccation cracks (Figure 1) or reactivate the preexisting inter-aggregate pores along former aggregate boundaries (Figure 3). The higher SOM content in the BL soil led to denser crack pattern in a drying emulsion (Figure 1) and to the formation of additional intra-aggregate pores through a higher number of new desiccation cracks with an aperture slightly bigger than the resolution limit. This SOM effect on crack pattern formation supports previous findings of (Zhang et al., 2016).

The clay-rich gleysol (GI) differed from the other two soils in that it had the highest SOM content, the highest clay content and the highest fraction of swelling clay minerals. In the drying emulsion this led to the densest crack pattern yet with smallest aperture which is consistent with the trend observed in RM and BL soil emulsions. In the structured soil this led to the largest formation of new intra-aggregate pores and to more pronounced changes in structure induced by drying. This is reflected by an increase in macroporosity and by a contraction of the soil matrix. The formation of desiccation cracks within former aggregates led to shorter pore distance in bulk soil at the same macroporosity as compared to the other two soils.

The general shape of the non-linear decrease in soil-pore distances and non-linear increase in connection probability Γ with increasing visible porosity due to drying and/or lower bulk density was similar for all three soils and was mainly imprinted by the same sieving and packing procedure. The roughly exponential decline in pore distances and steep Γ slope in the same macroporosity range supports previous results obtained with the aggregates that were sieved and repacked by the same protocol (Schlüter and Vogel, 2016). In cultivated top soils with a more irregular pore network formed by tillage and bioturbation the transition in Γ from many isolated pores to one dominating pore cluster is much more gradual across a wider porosity range and also more scattered (Jarvis et al., 2017; Pöhlitz et al., 2018; Schlüter et al., 2018). The general resemblance of the curves for cultivated soils and repacked soils could be due to the fact that plowing or harrowing leads to a similar soil structure like sieving and repacking.

Soil structure dynamics through wetting-drying cycles

The hypothesis was raised that natural soil structure turnover leads to a randomization of garnet particle locations with respect to pore distances over time (Schlüter and Vogel 2016). After packing, the particles used for aggregate coating tend to have short distances as many of them are directly exposed to the connected pore space. A thorough mixing of particles with soil through the destruction of old, coated pores and formation of new, uncoated pores should randomize their pore distances so that on the long run the mean particle-pore distance should approach the mean soil-pore distance, a state that is indicated with the 1:1 line in Figure 9. Soil structure dynamics induced by two wetting-drying cycles is clearly not sufficient to cause this randomization. This is because formation and closing of desiccation cracks is a very reversible process. Most cracks emerge in failure zones along former aggregate boundaries and are reactivated in subsequent drying cycles. It should be noted that the coating of aggregates with garnet particles itself might have somewhat biased the emergence of failure zones towards former aggregate boundaries. However, this reactivation of former aggregate boundaries also occurred where garnet particles were absent or sparse (compare Figure 3) and is also frequently observed in terms of crack reactivation in drying soil suspensions (Goehring et al., 2010; Wang et al., 2017). Some additional inter-aggregate pores were formed in the BL and GI through drying. This has the potential to expose previously occluded organic carbon to mineralization (Lopez-Sangil et al., 2018; Navarro-García et al., 2012), but our observations suggest that this effect is limited, since in the second drying event hardly any new cracks are formed. More importantly, garnet particles did not get more occluded with additional wetting-drying cycles beyond what was achieved during initial packing and wetting, because old failure zones get reactivated with every drying event. For substantial soil structure dynamics in the sense of a randomization of particle-pore distances the closure of cracks during wetting would need to be persistent and cracks would need to form at new locations during the next drying event. Altogether this suggests that substantial soil structure dynamics estimated through the randomization of passively translocated garnet particles is hardly noticeable in response to abiotic processes like wetting and drying but might be much more efficient with biotic processes like bioturbation or extreme soil structure changes induced by plowing. This will be investigated in future studies.

Conclusions

The magnitude of crack dynamics due to repeated wetting-drying cycles depended on a number of soil properties. The magnitude in macroporosity changes was largest in the clay-rich soil and was on average larger at the lower bulk density (1.22 g/cm³) than at the higher bulk density (1.48 g/cm³). A higher soil organic matter content led to a higher density of cracks with smaller aperture. In none of the investigated soils did the repeated wetting-drying cycles lead to a randomization of distances between garnet particles and pores. This soil structure dynamics is impaired by the fact that pre-existing failure zones are reinforced by repeated desiccation crack formation.

Acknowledgments

We are grateful to the editor and two anonymous reviewers for their helpful comments. This study was partially funded by the Deutsche Forschungsgemeinschaft through the research unit DFG-FOR 2337: Denitrification in Agricultural Soils: Integrated Control and Modelling at Various Scales (DASIM). We thank Jürgen Böttcher (Leibniz University Hannover, for sharing texture and organic matter data and Reinhold Jahn, Klaus Kaiser and Sonia Banze (Martin Luther University Halle-Wittenberg) for sharing clay mineralogy data for the RM and GI soil.

Literature

Altermann, M., Rinklebe, J., Merbach, I., Körschens, M., Langer, U., Hofmann, B., 2005. Chernozem—Soil of the Year 2005. J. Plant Nutr. Soil Sci. 168, 725–740. https://doi.org/10.1002/jpln.200521814

Baveye, P.C., Otten, W., Kravchenko, A., Balseiro-Romero, M., Beckers, É., Chalhoub, M., Darnault, C., Eickhorst, T., Garnier, P., Hapca, S., Kiranyaz, S., Monga, O., Mueller, C.W., Nunan, N., Pot, V., Schlüter, S., Schmidt, H., Vogel, H.-J., 2018. Emergent Properties of Microbial Activity in

Heterogeneous Soil Microenvironments: Different Research Approaches Are Slowly Converging, Yet Major Challenges Remain. Frontiers in Microbiology 9(1929), 1-48.
Beylich, A., Oberholzer, H.-R., Schrader, S., Höper, H., Wilke, B.-M., 2010. Evaluation of soil compaction effects on soil biota and soil biological processes in soils. Soil Tillage Res. 109, 133–143. https://doi.org/10.1016/j.still.2010.05.010
Borken, W., Matzner, E., 2009. Reappraisal of drying and wetting effects on C and N mineralization and fluxes in soils. Global Change Biology 15(4), 808-824.
Bottinelli, N., Jouquet, P., Capowiez, Y., Podwojewski, P., Grimaldi, M., Peng, X., 2015. Why is the influence of soil macrofauna on soil structure only considered by soil ecologists? Soil and Tillage Research 146, 118-124.
Darbon, J., Cunha, A., Chan, T.F., Osher, S., Jensen, G.J., 2008. Fast nonlocal filtering applied to electron cryomicroscopy. IEEE, pp. 1331–1334. https://doi.org/10.1109/ISBI.2008.4541250
de Mendiburu, F., 2019. Agricolae: statistical procedures for agricultural research, R package version.
Dexter, A.R., 1988. Advances in characterization of soil structure. Soil Tillage Res. 11, 199–238. https://doi.org/10.1016/0167-1987(88)90002-5
Dreibrodt, S., Kleber, M., & Jahn, R. (2002). Das Mineralinventar der Versuchsfläche "Statischer Dauerdüngungsversuch v120, Bad Lauchstädt". Archives of Agronomy and Soil Science, 48(3), 227-240. doi:10.1080/03650340213841
Fiès, J.C., Bruand, A., 1998. Particle packing and organization of the textural porosity in clay–silt–sand mixtures. European Journal of Soil Science 49(4), 557-567.
Goehring, L., Conroy, R., Akhter, A., Clegg, W.J., Routh, A.F., 2010. Evolution of mud-crack patterns during repeated drying cycles. Soft Matter 6, 3562. https://doi.org/10.1039/b922206e
Haas, C., Holthusen, D., Mordhorst, A., Lipiec, J., Horn, R., 2016. Elastic and plastic soil deformation and its influence on emission of greenhouse gases. Int. Agrophysics 30, 173–184. https://doi.org/10.1515/intag-2015-0088
Jarvis, N.J., 2007. A review of non-equilibrium water flow and solute transport in soil macropores: principles, controlling factors and consequences for water quality. European Journal of Soil Science 58, 523-546
Jarvis, N., Larsbo, M., Koestel, J., 2017. Connectivity and percolation of structural pore networks in a cultivated silt loam soil quantified by X-ray tomography. Geoderma 287, 71–79. https://doi.org/10.1016/j.geoderma.2016.06.026
Keiluweit, M., Wanzek, T., Kleber, M., Nico, P., Fendorf, S., 2017. Anaerobic microsites have an unaccounted role in soil carbon stabilization. Nat. Commun. 8. https://doi.org/10.1038/s41467-017-01406-6
Kittler, J., Illingworth, J., 1986. Minimum error thresholding. Pattern Recognition 19(1), 41-47.
Kögel-Knabner, I., Ekschmitt, K., Flessa, H., Guggenberger, G., Matzner, E., Marschner, B., von Lützow, M., 2008. An integrative approach of organic matter stabilization in temperate soils: Linking chemistry, physics, and biology. J. Plant Nutr. Soil Sci. 171, 5–13. https://doi.org/10.1002/jpln.200700215
Köhne, J.M., Köhne, S., Simunek, J., 2009. A review of model applications for structured soils: a) Water flow and tracer transport. Journal of Contaminant Hydrology 104, 4-35.
Kravchenko, A.N., Guber, A.K., 2017. Soil pores and their contributions to soil carbon processes. Geoderma 287, 31–39. https://doi.org/10.1016/j.geoderma.2016.06.027
Kuzyakov, Y., Blagodatskaya, E., 2015. Microbial hotspots and hot moments in soil: Concept & review. Soil Biol. Biochem. 83, 184–199. https://doi.org/10.1016/j.soilbio.2015.01.025
Legland, D., Arganda-Carreras, I., Andrey, P., 2016. MorphoLibJ: integrated library and plugins for mathematical morphology with ImageJ. Bioinformatics btw413. https://doi.org/10.1093/bioinformatics/btw413
Lehmann, J., Kleber, M., 2015. The contentious nature of soil organic matter. Nature. https://doi.org/10.1038/nature16069

Lopez-Sangil, L., Hartley, I.P., Rovira, P., Casals, P., Sayer, E.J., 2018. Drying and rewetting conditions differentially affect the mineralization of fresh plant litter and extant soil organic matter. Soil Biol. Biochem. 124, 81–89. https://doi.org/10.1016/j.soilbio.2018.06.001

Navarro-García, F., Casermeiro, M.Á., Schimel, J.P., 2012. When structure means conservation: Effect of aggregate structure in controlling microbial responses to rewetting events. Soil Biol. Biochem. 44, 1–8. https://doi.org/10.1016/j.soilbio.2011.09.019

Ollion, J., Cochennec, J., Loll, F., Escudé, C., Boudier, T., 2013. TANGO: a generic tool for high-throughput 3D image analysis for studying nuclear organization. Bioinformatics 29, 1840–1841. https://doi.org/10.1093/bioinformatics/btt276

Pöhlitz, J., Rücknagel, J., Koblenz, B., Schlüter, S., Vogel, H.-J., Christen, O., 2018. Computed tomography and soil physical measurements of compaction behaviour under strip tillage, mulch tillage and no tillage. Soil Tillage Res. 175, 205–216. https://doi.org/10.1016/j.still.2017.09.007

Rabot, E., Wiesmeier, M., Schlüter, S., Vogel, H.-J., 2018. Soil structure as an indicator of soil functions: A review. Geoderma 314, 122–137. https://doi.org/10.1016/j.geoderma.2017.11.009

Renard, P., Allard, D., 2013. Connectivity metrics for subsurface flow and transport. Advances in Water Resources 51(0), 168-196.

Schindelin, J., Arganda-Carreras, I., Frise, E., Kaynig, V., Longair, M., Pietzsch, T., Preibisch, S., Rueden, C., Saalfeld, S., Schmid, B., Tinevez, J.-Y., White, D.J., Hartenstein, V., Eliceiri, K., Tomancak, P., Cardona, A., 2012. Fiji: an open-source platform for biological-image analysis. Nat. Methods 9, 676–682. https://doi.org/10.1038/nmeth.2019

Schlüter, S., Großmann, C., Diel, J., Wu, G.-M., Tischer, S., Deubel, A., Rücknagel, J., 2018. Long-term effects of conventional and reduced tillage on soil structure, soil ecological and soil hydraulic properties. Geoderma 332, 10–19. https://doi.org/10.1016/j.geoderma.2018.07.001

Schlüter, S., Sheppard, A., Brown, K., Wildenschild, D., 2014. Image processing of multiphase images obtained via X-ray microtomography: A review. Water Resour. Res. 50, 3615–3639. https://doi.org/10.1002/2014wr015256

Schlüter, S., Vogel, H.-J., 2016. Analysis of Soil Structure Turnover with Garnet Particles and X-Ray Microtomography. PLOS ONE 11, e0159948. https://doi.org/10.1371/journal.pone.0159948

Smith, K.A., Ball, T., Conen, F., Dobbie, K.E., Massheder, J., Rey, A., 2003. Exchange of greenhouse gases between soil and atmosphere: interactions of soil physical factors and biological processes. Eur. J. Soil Sci. 54, 779–791. https://doi.org/10.1046/j.1351-0754.2003.0567.x

Totsche, K.U., Amelung, W., Gerzabek, M.H., Guggenberger, G., Klumpp, E., Knief, C., Lehndorff, E., Mikutta, R., Peth, S., Prechtel, A., Ray, N., Kögel-Knabner, I., 2018. Microaggregates in soils. Journal of Plant Nutrition and Soil Science 181(1), 104-136.

Wang, C., Zhang, Z., Liu, Y., Fan, S., 2017. Geometric and fractal analysis of dynamic cracking patterns subjected to wetting-drying cycles. Soil Tillage Res. 170, 1–13. https://doi.org/10.1016/j.still.2017.02.005

Wang, C., Zhang, Z.-y., Fan, S.-m., Mwiya, R., Xie, M.-x., 2018. Effects of straw incorporation on desiccation cracking patterns and horizontal flow in cracked clay loam. Soil and Tillage Research 182, 130-143.

Wilcke, W., Kaupenjohann, M., 1997. Differences in concentrations and fractions of aluminum and heavy metals between aggregate interior and exterior. Soil science 162(5), 323-332.

Young, I.M., 2004. Interactions and Self-Organization in the Soil-Microbe Complex. Science 304, 1634–1637. https://doi.org/10.1126/science.1097394

Young, I.M., Crawford, J.W., Nunan, N., Otten, W., Spiers, A., 2008. Chapter 4 Microbial Distribution in Soils: Physics and Scaling. Academic Press, pp. 81-121.

Zhang, Z.B., Zhou, H., Lin, H., Peng, X., 2016. Puddling intensity, sesquioxides, and soil organic carbon impacts on crack patterns of two paddy soils. Geoderma 262, 155–164. https://doi.org/10.1016/j.geoderma.2015.08.030